# A Numerical Study of the Effects of Narrow Channel Dimensions on Pressure Drop and Mass Transfer Performance of a Mixer Device

***Fatima, Urooj****[+]

*Department of Chemical Engineering, NED University of Engineering and Technology, Karachi, PAKISTAN*

***Shakaib, Muhammad***

*Department of Mechanical Engineering, NED University of Engineering and Technology, Karachi, PAKISTAN*

**ABSTRACT:** *The numerical study in this paper investigates the effect of inlet and outlet areas of micromixer channels on fluid flow behavior and mass transfer performance. The ratio of the outlet to the junction area is varied from 0.6−2 while the ratio of the inlet to junction area is from 0.6−1.4. The flow patterns obtained for various mixers indicate that vortices or recirculation zones are created as the two fluids turn and enter the outlet channel. The formation of recirculation regions results in enhanced mixing rates. The micromixers are evaluated in terms of mixing quality, pressure drop, and mixing effectiveness parameters. The mixing quality increases up to 10 times when the outlet area ratio increases from 0.6 to 2. The rise in pressure drop due to the increased outlet area is about 50%. The inlet area also influences the mixing rate and pressure drop. The mixing quality first increases and then decreases with an increase in area. The pressure drop, whereas, continuously decreases when the inlet area ratio increases from 0.6 to 1.4. Suitable dimensions of micromixers are suggested based on mixing effectiveness. A mixer device with an outlet/junction area ratio of 1.2 and an inlet/junction area ratio 0.8−1 is found to provide better performance.*

**KEYWORDS:** *Computational Fluid Dynamics (CFD); Micromixer; Mixing quality; Pressure drop mixing effectiveness.*

## INTRODUCTION

Microfluidic systems are widely used in the scientific fields of chemical, biomedical, pharmaceutical, and materials science [1-5]. An integral component in these systems is the micromixer which fulfills the mixing requirements of important processes such as organic synthesis, polymerization, DNA analysis, protein folding, and enzyme reactions [6-10]**.** Micromixers are of an active or passive type. The passive type is generally preferred due to the ease of designing, fabrication, and integration with the external microfluidic system. A limitation of a passive micromixer is that laminar flow conditions are prevalent and the rate of mixing is relatively low. Several studies, therefore, have proposed geometrical modifications to create secondary flows that reduce the diffusion length and enhance mixing.

Due to advancements in computational methods and

***** *To whom correspondence should be addressed.*
*+ E-mail: mshakaib@neduet.edu.pk*
*1021-9986/2022/5/1727-1739 13/$/6.03*

resources, Computational Fluid Dynamics (CFD) now is an effective tool for understanding complex hydrodynamics and designing various flow systems [11, 12]. CFD technique has been utilized to examine the flow and mixing behavior in mixer devices also. *Gobby et al.* [13] studied the effect of confluence angle and throttling at the junction of a T-shaped microchannel. The authors found that the throttling decreases the mixing length and enhances the mixing performance. *Soleymani et al.* [14] examined the effect of throttle size, aspect ratio, and mixing angle and showed that these parameters strongly affect secondary flow development and mixing behavior. The numerical work of *Su et al.* [15] on angled micromixers revealed that mixing efficiency is inversely related to channel width and flow velocity**.** *Darbandi et al.* [16] studied throttle mixers with varying widths and shapes and reported that the mixing length decreases with a decrease in throttle width. An analysis of L and V-shaped micromixers in 3D space was carried out by *Zare et al.* [17]. The L-shaped micromixers had better mixing performance than the V-shaped micromixers. The experimental and numerical study of *Wong et al.* [18] indicated that at an inlet pressure of 5.5 bars (or higher), the fluids mix within a millisecond after they come in contact. The experimental investigations of *Silva et al.* [19] found that the asymmetric fluid flow conditions in a mixing device are beneficial for improved mass transfer performance**.** Micro laser-imaging and particle imaging velocimetry techniques were used by *Hoffmann et al.* [20] to visualize the flow and the mixing characteristics. It was found that at a certain value of Reynolds number, the flow regime changes from stratified/vortex to engulfment. The present authors studied fluid flow and mass transfer in mixer channels and proposed suitable confluence angles for micromixer devices [21]. In addition to relatively simple geometries, several other complex designs have been recommended by researchers such as micromixers with stirrers [22] with obstructions [23-25] or with complex internal structures [26-28]. Many of these micromixer types, however, are difficult to fabricate and integrate with the other microsystem components. The review of the literature shows that several studies have been performed to investigate the flow and the mixing characteristics of micromixers. These studies show that geometric parameters like confluence angle and width-to-height aspect ratios influence mixing efficiency. To the authors' knowledge, the variation of area ratio that is the inlet to the junction area and similarly, the outlet to the junction area has not been examined in detail. In the present work, therefore, T-shaped mixers with varying dimensions of inlet and outlet channels are considered. The simulations are conducted at different Reynolds numbers and based on calculations of mixing parameters appropriate widths of inlet and outlet channels are indicated.

## THEORETICAL SECTION

### *Modeling*

CFD analysis is carried out for the study of flow behavior and mass transfer in mixer channels. The dimensions such as length, width, and height of micromixer channels can differ due to a variety of applications. In the present work, T-shaped mixers with typical channel dimensions are considered. The schematic for the micromixer device is shown in Fig. 1. The channel height $h$ and the width at junction $w_j$ are constant and equal to 400 microns. The widths of the inlet channels $w_i$ and the outlet channel $w_o$ and thus the inlet and the outlet channel areas $A_i$ and $A_o$, respectively are variable. The ratios of $A_i$ and $A_o$ per unit junction area $A_j$ are denoted as $R_i$ and $R_o$, respectively. The lengths of both inlets and outlet channels are 6000 microns. The channel area ratios studied in this paper are given in Table 1. Water is supplied from one of the mixer inlets while tracer/due solution is supplied from the other. The characteristics of fluids used in micromixers often have the same properties. The density $\rho$ and viscosity $\mu$ of water and the dye solution (tracer) is thus assumed the same and the values are 998 kg/m$^3$ and 0.001 kg/m·s, respectively. The diffusivity of the tracer in water is $1.5 \times 10^{-9}$ m$^2$/s which results in a Schmidt number of 650.

A structured mesh is created for the CFD analysis as shown in Fig. 2. In the mixing zone (i.e. at the junction) and adjacent to the walls the mesh/grid density is higher. The mesh cells gradually increase in size away from the junction. To ensure that the results are grid-independent, a preliminary convergence study is carried out. The mixing quality calculated for a case at different grids is shown in Fig. 3. An optimal mesh of 8.5 x $10^5$ is chosen based on a tradeoff between the calculation time and the accuracy of the solution. The gravitational effect is ignored by assuming the micromixer is in a horizontal orientation. Velocity is specified at the inlet for water and tracer fluids. At the exit, the pressure is set to 0 Pa.

***Table 1: Micromixer geometries/channel area ratios considered in this work.***

| | | | | | | | | | | | | |
|---|---|---|---|---|---|---|---|---|---|---|---|---|
| Inlet / Junction Area Ratio $R_i$ | 1 | 1 | 1 | 1 | 1 | 1 | 1 | 1 | 0.6 | 0.8 | 1.2 | 1.4 |
| Outlet / Junction Area Ratio $R_o$ | 1 | 0.6 | 0.8 | 1.2 | 1.4 | 1.6 | 1.8 | 2 | 1 | 1 | 1 | 1 |

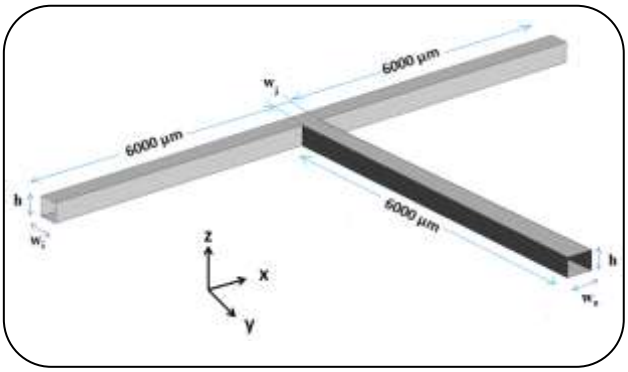


***Fig. 1: Geometry and computational domain for micromixers.***

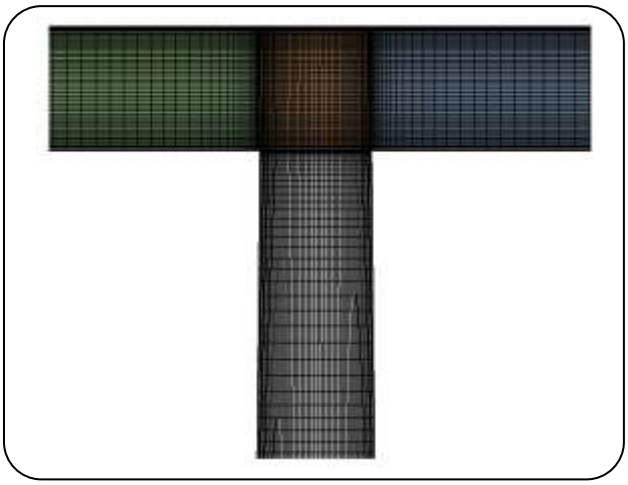

***Fig. 2: Cross-sectional top view of mesh used for a micromixer ($R_o$ = 1.4, $R_i$ = 1).***

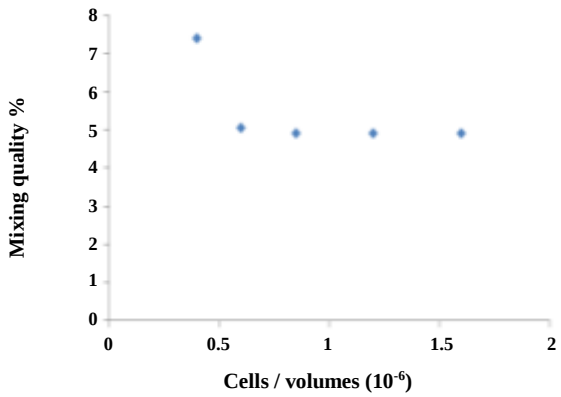


***Fig. 3. Grid independence study for a T-shaped micromixer ($R_o$ = $R_i$ = 1, Re = 260).***

The remaining surfaces are impermeable walls on which no-slip conditions are imposed. The governing equations for steady, laminar, and isothermal flow which includes species transport without reaction are continuity, momentum, and concentration equations as given in Equations (1-5):

$$\frac{\partial u}{\partial x}+\frac{\partial v}{\partial y}+\frac{\partial w}{\partial z}=0 \tag{1}$$

$$u\frac{\partial u}{\partial x}+v\frac{\partial u}{\partial y}+w\frac{\partial u}{\partial z}= -\frac{1}{\rho}\frac{\partial p}{\partial x}+v\left(\frac{\partial^2 u}{\partial x^2}+\frac{\partial^2 u}{\partial y^2}+\frac{\partial^2 u}{\partial z^2}\right) \tag{2}$$

$$u\frac{\partial v}{\partial x}+v\frac{\partial v}{\partial y}+w\frac{\partial v}{\partial z}= -\frac{1}{\rho}\frac{\partial p}{\partial y}+v\left(\frac{\partial^2 v}{\partial x^2}+\frac{\partial^2 v}{\partial y^2}+\frac{\partial^2 v}{\partial z^2}\right) \tag{3}$$

$$u\frac{\partial w}{\partial x}+v\frac{\partial w}{\partial y}+w\frac{\partial w}{\partial z}= -\frac{1}{\rho}\frac{\partial p}{\partial z}+v\left(\frac{\partial^2 w}{\partial x^2}+\frac{\partial^2 w}{\partial y^2}+\frac{\partial^2 w}{\partial z^2}\right) \tag{4}$$

$$u\frac{\partial m_A}{\partial x}+v\frac{\partial m_A}{\partial y}+w\frac{\partial m_A}{\partial z}= D_{AB}\left(\frac{\partial^2 m_A}{\partial x^2}+\frac{\partial^2 m_A}{\partial y^2}+\frac{\partial^2 m_A}{\partial z^2}\right) \tag{5}$$

The equations are solved using CFD code ANSYS Fluent. The second-order upwind scheme is used for the discretization of momentum and concentration/mass transfer equations and SIMPLE (Semi-Implicit Method for Pressure Linked Equations) algorithm is used to couple pressure and velocity fields [29]. The convergence criterion for residuals of continuity, momentum, and mass fraction is set equal to $10^{-5}$.

The flow in microfluidic devices is usually laminar. The simulations are therefore conducted at Reynolds numbers which are in the laminar range i.e. 20, 100, 180, and 260. The Reynolds number is defined as:

$$\mathrm{Re} = \frac{u_{av} d}{v} \tag{6}$$

Where $u_{av}$ is the average velocity in the mixing (outlet) channel, $d$ is hydraulic diameter and $v$ is kinematic viscosity. The hydraulic diameter is defined in Eq. (7) where $h$ is the height of the channel and $w_{av}$ is the average width of the outlet channel.

$$d = \frac{4(h \times w_{av})}{2(h \times w_{av})} \tag{7}$$

$$w_{av} = \frac{w_j + w_o}{2} \tag{8}$$

The flow characteristics are also explained in terms of vorticity along the mixing channel. For this purpose, a related quantity termed circulation $\omega_y$is determined.

$$\omega_y = \int\left(\frac{\partial w}{\partial x} - \frac{\partial u}{\partial z}\right) dx\, dz \tag{9}$$

The mixing is characterized using a volumetric-based mixing quality $\alpha$ as proposed by *Lobasov et al.* [30]:

$$\alpha = 1 - \sqrt{\frac{\sigma^2}{\sigma_0^2}} \tag{10}$$

Where $\sigma$ is the standard deviation of the mass fraction of the tracer from its mean value $\overline{m}_A$ whereas $\sigma_0$ is the maximum standard deviation of the mass fraction of the tracer $m_A$. $\sigma$ and $\sigma_0$ are calculated using Eqs (11) and (12) respectively

$$\sigma^2 = \frac{1}{V}\int\left(m_A - \overline{m}_A\right)^2 dV \tag{11}$$

Where $V$ is the volume of the computational domain.

$$\sigma_0^2 = \overline{m}_A\left(1 - \overline{m}_A\right) \tag{12}$$

In the case of complete mixing $\alpha = 1$ whereas $\alpha = 0$ means no mixing.

Suitable designs of micromixers are proposed based on 'Mixing effectiveness' (ME) which is a ratio of mixing quality and Euler number $\Delta p/\rho u^2$ as given in Eq. (13)

$$\mathrm{ME} = \frac{\alpha}{\mathrm{Eu}} \tag{13}$$

For evaluation, the present results are compared qualitatively with the work of *Hoffmann et al.* [20]. The quantitative comparison is done by determining the friction factor from pressure drop and segregation index using the standard deviation of the mass fraction at various sections in the mixing channel. The comparison is done with the work of *Aoki et al.* [2, 3]. The relations for friction factor $f$ and segregation index SI are:

$$f = \frac{\Delta p\, d}{L}\frac{2}{\rho u_{av}^2} \tag{14}$$

$$\mathrm{SI} = \frac{\sigma}{\sigma_0} \tag{15}$$

## RESULTS AND DISCUSSION

The velocity and the mass fraction contours in micromixers with different $R_o$ ratios are shown in Fig. 4. The velocity profiles indicate that as the outlet area ratio $R_o$ increases, the local velocity in the center of the mixing channel increases. Since the Reynolds number is the same in all the cases, the increment of velocity magnitude in the center increases the size of the low-velocity region at the corners of the mixing channels. The mass fraction contours are also affected by the change in outlet channel width $w_o$ (or $R_o$ ratio). When $R_o$ is small, the variation of mass fractions is only observed in a thin region. At large $R_o$ ratios (such as $R_o$ = 1.4–2) local mass fractions are found to be varying more.

The fluid flow in the mixing channel is mainly in the $y$-direction i.e. the $v$-velocity is the major component. The magnitudes of $u$ and $w$ velocity components, however, increase as the fluids take a sharp turn at the junction of the inlets and the mixing channels. The velocity vector plots, thus, as shown in Fig. 5 show recirculation zones of considerable size. A comparison of different mixers indicates that velocity has relatively high magnitudes when the mixing channel has a large area (or $R_o$ value). In mixers with large area ratios particularly when $R_o$ = 1.8 or 2, a region is also noticed in which the velocity vectors appear as dots. This means that the flow is axial in this region.

To predict the intensity of rotational movement and its variation with the mixing channel, circulation $\omega_y$ is calculated and shown in Fig. 6a. The circulation is a maximum at the beginning of the mixing channel due to a major change in the fluid direction. It then decreases as the two fluids streamline while flowing toward the outlet section. The circulation plots versus distance also indicate that

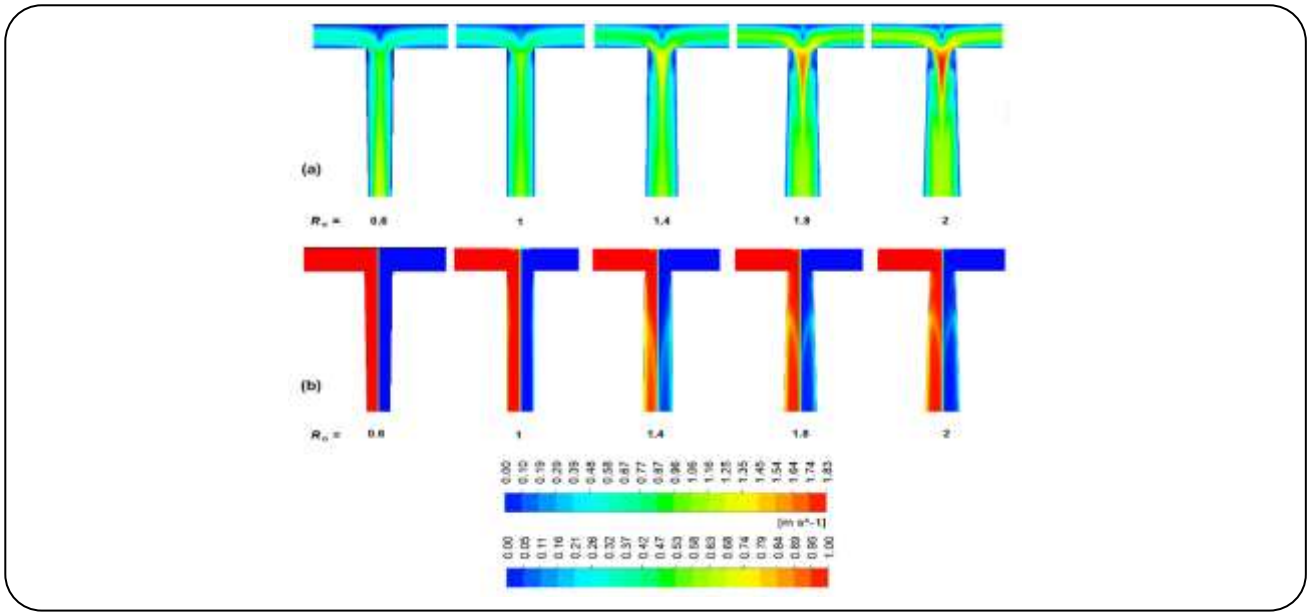


***Fig. 4: Contours of velocity and mass fraction of tracer in different micromixers ($R_i$ = 1, Re = 260).***

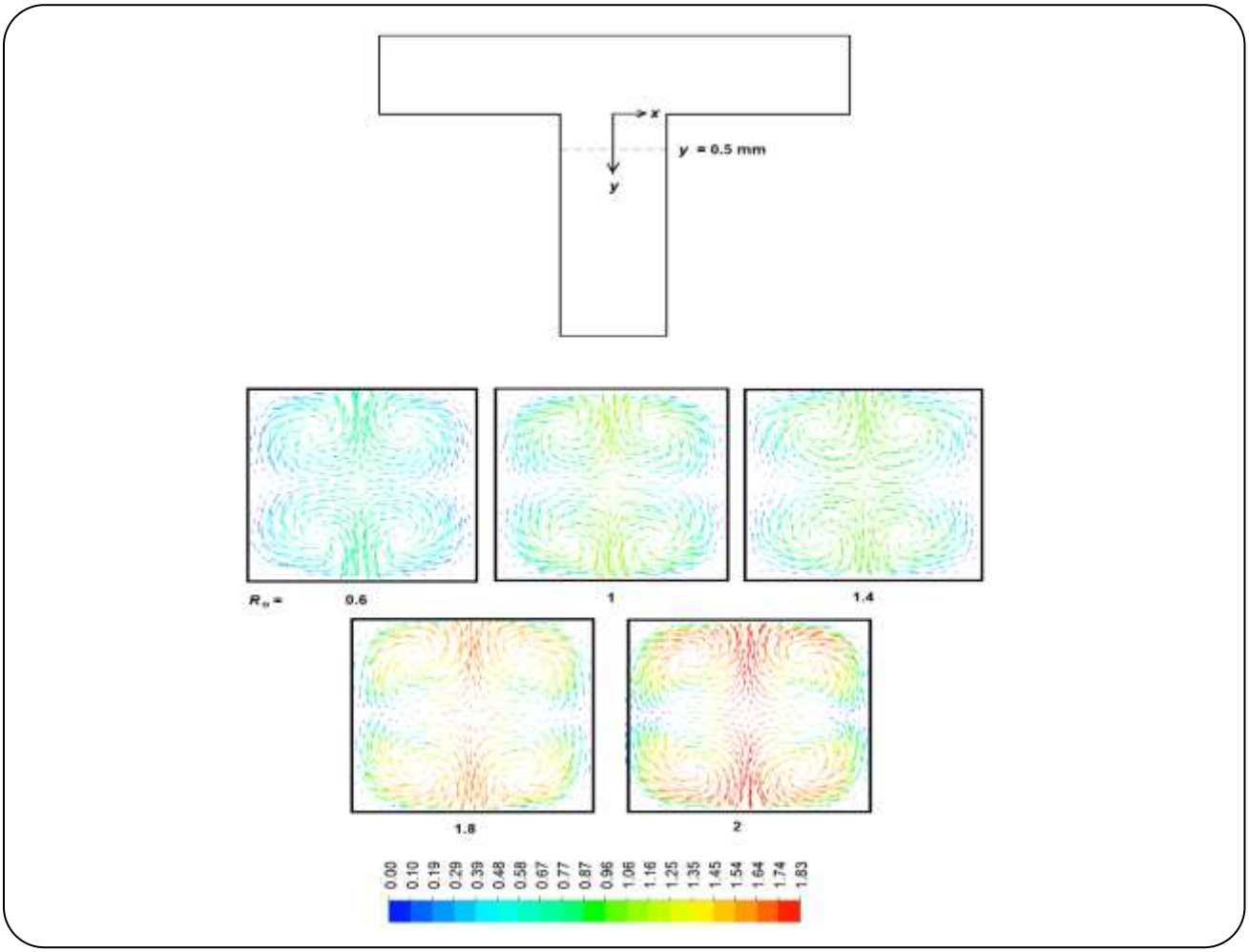


***Fig. 5: Velocity vectors in mixers with different Ro at y = 0.5 mm (Re =260).***

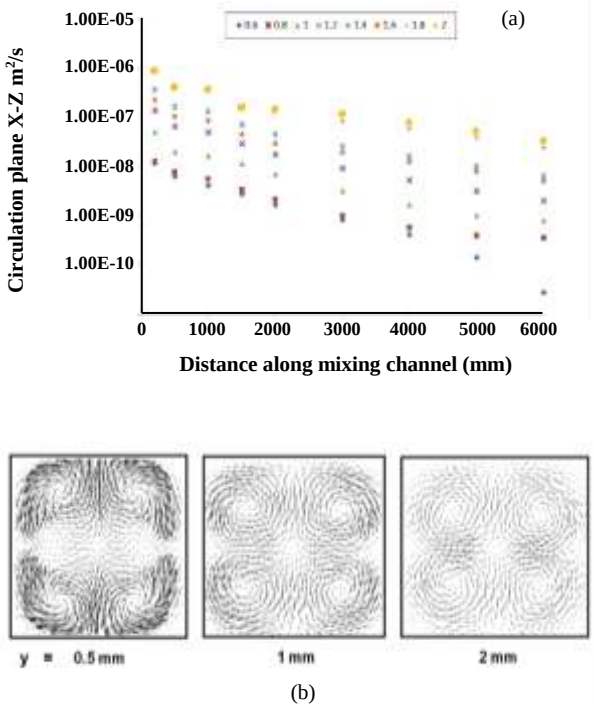


***Fig. 6: (a) Variation of circulation along the mixing channel (b) velocity vectors for a mixer with $R_o$ = 2 at y = 0.5, 1, and 2 mm.***

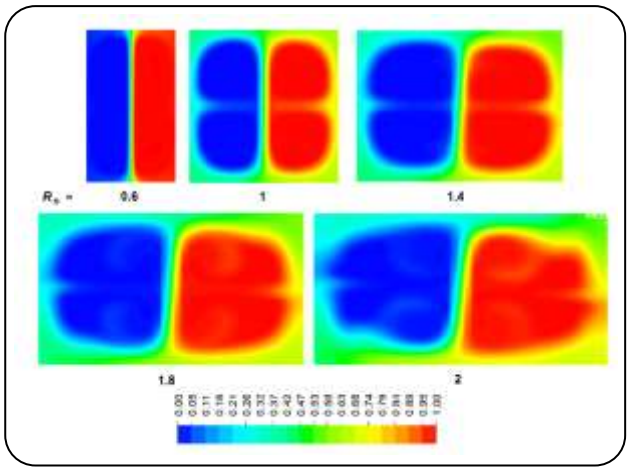


***Fig. 7: Concentration contours (at outlet cross-section) for different $R_o$ (Re = 260).***

the flow rotations generally increase with an increase in $R_o$. The reason is that the mixers with a large $R_o$ ratio have large diverging angles (as the junction area $A_j$ or width $w_j$ is the same). The diverging channel allows more space for the formation of vortices. The circulation behavior in velocity vector form is given for one of the geometries ($R_o$ = 2) in Fig. 6b. The vectors at different $y$ locations reveal significant fluid motion in the transverse plane at $y$ = 0.5 mm. As the fluid moves ahead toward the outlet section, the strength of vortices is reduced and the flow direction becomes mostly axial (i.e. $u \approx 0$, $w \approx 0$) as can be seen in the plane of $y$ = 2 mm. The mass fraction/concentration contours in Fig. 7 show that the mixing of two fluids streams is restricted only in the thin interface region when $R_o$ = 0.6. At large $R_o$ ratios, for example, $R_o \geq 1$, the regions of the mixed fluids layer (which have an average mass fraction value of about 0.5 kg/kg) are found at the central interface as well as at the channel's walls. When $R_o \geq 1.4$, the contours are observed as asymmetric in the horizontal ($xy$-plane). This is due to the presence of high-velocity vortices previously seen in Fig. 5.

The effect of the inlet area ratio ($R_i = A_i/A_j$) on the circulation component $\omega_y$ is shown in Fig. 8. The Figure shows that when $R_i$ is 0.8 or 1.0, the circulation values are high, in particular, up to a distance of 2000 μm. The circulation then decreases rapidly with distance/length along the mixing channel. The circulation in channels with a large inlet area (i.e. $R_i$ = 1.2 or 1.4) is relatively less which means the flow is almost stabilized or less rotational. Similarly in the geometry with small $R_i$ ($R_i$ = 0.6), flow turning into the mixing channel is fairly smooth which results in low circulations at different locations.

The circulation or formation of vortices in mixer narrow channels directly affects the mass transfer process as can be seen in Fig. 9. The mass fraction contours at the exit section illustrate that the mixed region (in which $m_A \approx 0.5$) is in the middle vertical plane of the channel and near the walls in cases of $R_i$ = 0.8, 1.0 or 1.2. When $R_i$ is small or large (0.6 or 1.4, respectively), the mass fraction profile shows water and tracer as almost segregated streams due to inappreciable flow rotations.

The quantitative results for mixing quality ($\alpha$) and pressure drop ($\Delta p$) are shown in Fig. 10. The trend of $\alpha$ versus $Re$, for most of the geometries (i.e. $R_o \geq 0.8$), shows that mixing quality increases with the Reynolds number. This is due to the fact that the dominant mixing phenomenon at a low Reynolds number is molecular diffusion while at a high Reynolds number the secondary flow structures facilitate the intermingling of the fluid streams. In the case of $R_o$ = 0.6, the mixing qualities are very low due to smooth and streamlined flow.

Since there is a sufficient rise in mixing quality with the Reynolds number, the flow in mixers with $R_o \geq 0.8$ can be within the vortex or the engulfment regime.

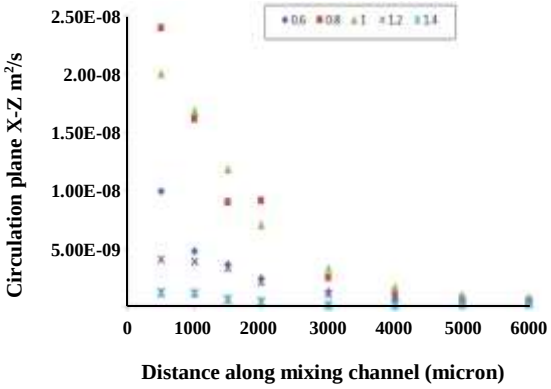


***Fig. 8: Circulation along the mixing channel for different $R_i$ (Re = 260).***

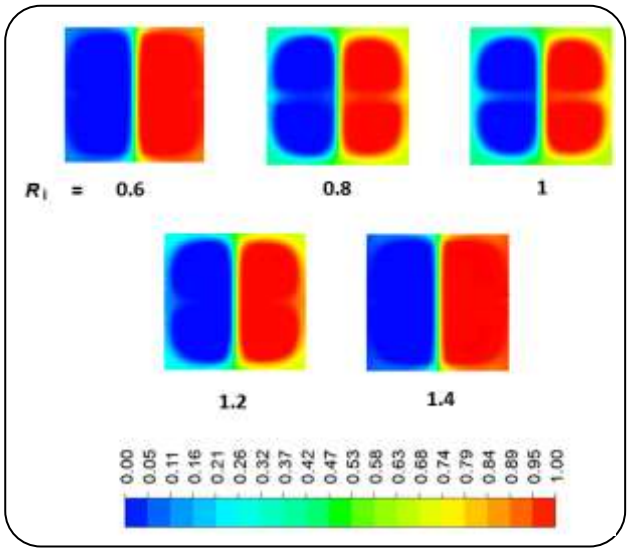


***Fig. 9: Concentration contours (at outlet cross-section) for different $R_i$ (Re = 260).***

The plot in Fig. 10(b) shows that the micromixers with $R_i$ = 0.8 or 1 which results in more circulation (as observed in Fig. 8) are found to yield high mixing qualities. In the mixer with a small $R_i$ ratio of 0.6, the mixing process is restricted due to more viscous effects in the inlet channel. Similarly, in the cases of large $R_i$ (i.e. 1.2 or 1.4), the movement of fluids from a large area into a narrow region decreases flow rotation and limits the mixing process. The mixing quality is thus low in these mixer geometries.

The increase in Reynolds number increases shear drag at the mixer walls and form drag due to a sudden change in the flow direction. The pressure drops thus simply increase with an increase in Reynolds number as expected. When the outlet area is small ($R_o$ = 0.6) the viscous loss is more whereas the loss due to flow circulation is low. As $R_o$ increases ($R_o$ = 0.8 or 1) the viscous loss decreases while loss associated with circulation or change in flow direction increases. The total pressure drop at any Reynolds number hence remains almost the same when $0.6 \leq R_o \leq 1$. Further enlargement of the mixing channel area (i.e. $R_o > 1$) does not reduce viscous loss much but increases the size of the separation or recirculation region. This in turn increases the hydraulic / pressure drop. The increase in area ratio ($R_i$ or $A_i$ /$A_j$) reduces friction which decreases the pressure drop which can clearly be observed in Fig. 10d. As the pressure drop has a direct relation with Reynolds number and outlet area ratio and an inverse relation with $R_i$, a simple correlation is developed and given in equation (16). It can be used to predict pressure drops in T-shaped mixers.

$$\Delta p = 5.21 \mathrm{Re}^{1.16} \mathrm{R}_o^{0.33} \mathrm{R}_i^{-0.69} \qquad (16)$$

The mixing effectiveness (ME) is calculated using equation (13) and shown in Fig. 11. Since dimensionless pressure drop ($\Delta p/\rho u^2$) drops due to an increase in velocity or Reynolds number, the increase in Reynolds number considerably increases mixing effectiveness (ME). The effect of area ratio $R_o$ in Fig. 11(a) shows that for $R_o$ = 0.6, the rise in ME with Reynolds number is less rapid in comparison to others. The optimal area ratio $R_o$ for the mixer based on mixing effectiveness depends on the Reynolds number. At a Reynolds number of 100, the mixing effectiveness is found to be high when $R_o$ = 2. At high Reynolds numbers of 180 or 260, the mixers with large $R_o$ ($\geq$ 1.4) result in high-pressure drops as previously seen in Fig.10(c). A geometry with $R_o$ = 1.2, which has a reasonable value of mixing quality with moderate pressure drop results in maximum effectiveness. The micromixers with $R_o$ close to 1.2 can be considered superior in terms of mixing effectiveness parameters. The curves of ME for different $R_i$ indicate that the effectiveness, similar to mixing quality is found high when $R_i$ = 0.8 or 1. This suggests that varying the dimensions/area ratio of the inlet channel from unity does not have any useful effect on the mixing process.

The mixing rates in micromixers are related to the various laminar flow regimes (stratified, vortex, and engulfment) as known from previous literature. The types of mass fraction/concentration profiles observed depending on the flow regime are further examined and depicted in Fig. 12. The Figure shows

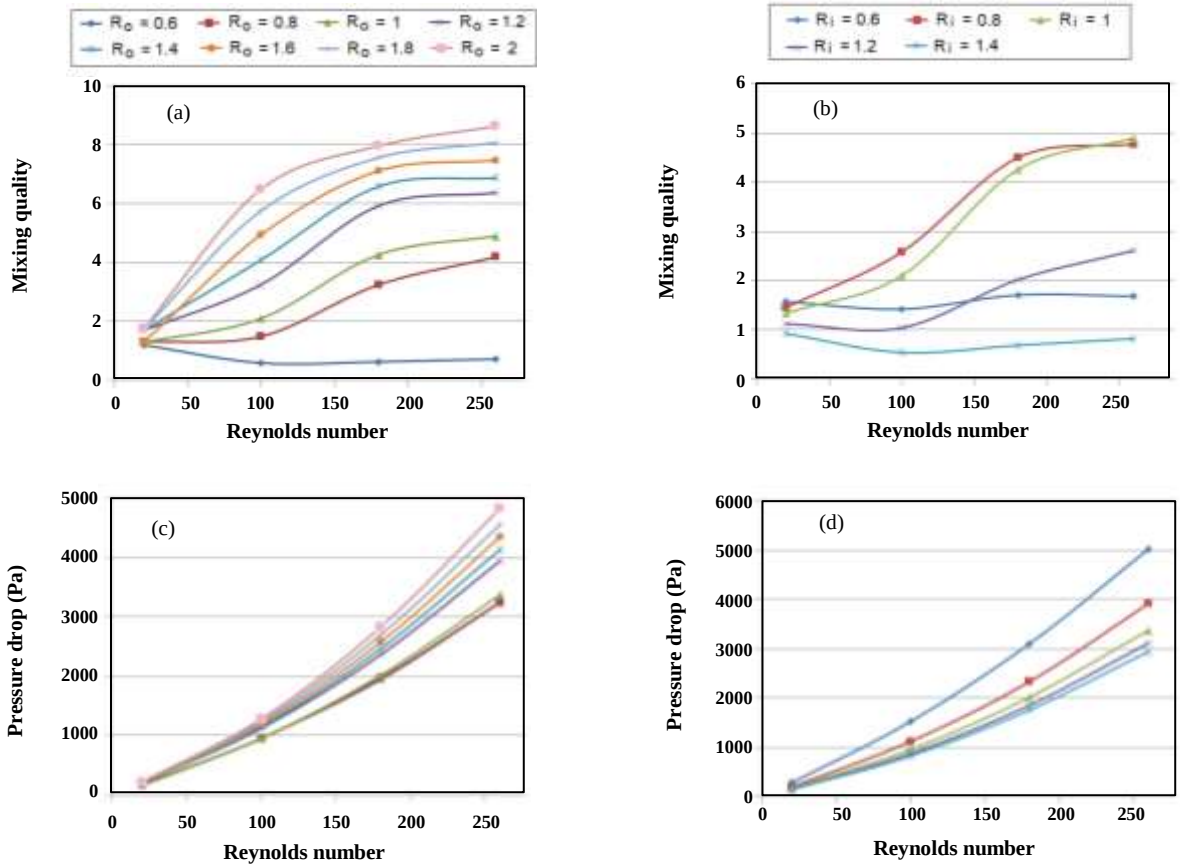


***Fig. 10: (a,b) Mixing quality and (c,d) pressure drop versus Reynolds number for different area ratios $R_o$ and $R_i$ .***

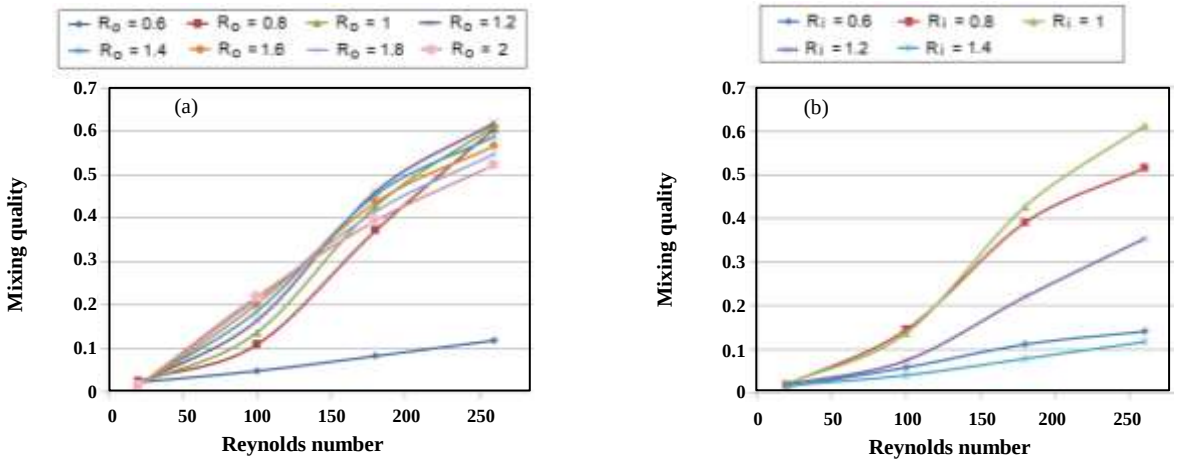


***Fig. 11: Effect of Reynolds number and area ratios (a) $R_o$ and (b) $R_i$ on mixing effectiveness.***

three types of profiles in which (a)tracer-water mixing is found only in the thin central portion, (b) mixed layers are present in the vertical central region and at wall boundaries, or (c) asymmetric mass fraction distribution is seen. The three types of profiles are due to stratified, vortex, and engulfment regimes, respectively. The comparison of these profiles with the calculated mixing quality reveals that the mixing quality is low when the flow is stratified. It increases in the vortex regime and then further increases in the engulfment range.

***Table 2: Reynolds number ranges for the flow regimes in different micromixers.***

| Mixer Geometry/ Flow Regimes | Stratified | Vortex | Engulfment |
|---|---|---|---|
| $R_i = 0.6$, $R_o = 1$ | $Re \leq 260$ | --- | --- |
| $R_i = 0.8$, $R_o = 1$ | $Re \leq 100$ | $100 < Re \leq 260$ | --- |
| $R_i = 1$, $R_o = 1$ | $Re \leq 100$ | $100 < Re \leq 260$ | --- |
| $R_i = 1.2$, $R_o = 1$ | $Re \leq 100$ | $100 < Re \leq 260$ | --- |
| $R_i = 1.4$, $R_o = 1$ | $Re \leq 260$ | --- | --- |
| $R_i = 1$, $R_o = 0.6$ | $Re \leq 260$ | --- | --- |
| $R_i = 1$, $R_o = 0.8$ | $Re \leq 100$ | $100 < Re \leq 260$ | --- |
| $R_i = 1$, $R_o = 1.2$ | $Re \leq 100$ | $100 < Re \leq 180$ | $Re > 180$ |
| $R_i = 1$, $R_o = 1.4$ | $Re \leq 100$ | $100 < Re \leq 180$ | $Re > 180$ |
| $R_i = 1$, $R_o = 1.6$ | $Re \leq 20$ | $20 < Re \leq 180$ | $Re > 180$ |
| $R_i = 1$, $R_o = 1.8$ | $Re \leq 20$ | $20 < Re \leq 180$ | $Re > 180$ |
| $R_i = 1$, $R_o = 2$ | $Re \leq 20$ | $20 < Re \leq 180$ | $Re > 180$ |

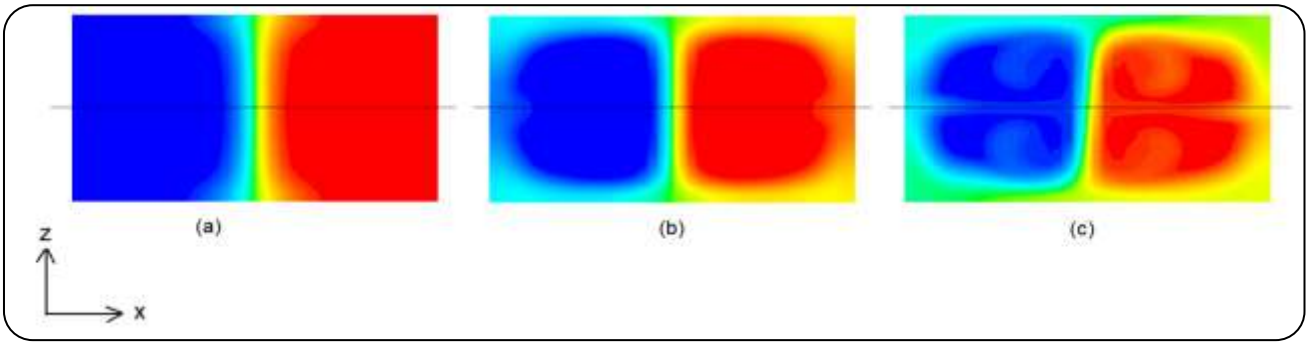


***Fig. 12: Mass fraction contours at the exit for (a) stratified (b) vortex (c) engulfment flow ($R_o$ = 1.4).***

The Reynolds number at which the transition to engulfment takes place depends on the type of geometry. In the present work, from the evaluation of mass fraction distribution, the ranges of Reynolds numbers in which the three regimes that exist are identified. Table 2 shows that when the area ratio $R_i$ is low or high (i.e. 0.6 or 1.4) the flow is stratified in the entire range of Reynolds numbers considered in this study. When $0.8 \leq R_i \leq 1.2$, vortex flow takes place when the Reynolds number is 180 and 260. The ranges for $R_o$ indicate that the flow remains stratified up to Re = 260 when $R_o$ = 0.6. When Ro is 0.8 or 1, the regime is stratified up to Re = 100 and vortex flow is seen when Re = 180 or 260. The engulfment regime that is the asymmetric mass fraction distribution is only observed when $R_o \geq 1.2$ and the Reynolds number is 260.

The critical Reynolds number for the engulfment flow is obtained from the degree of asymmetry found in the mass fraction contours. In the cases of stratified and vortex flow, the top and bottom portions of mass fraction contours are exactly the same. In the engulfment regime, the distribution is non-uniform about *xy* plane and the average concentration in the top and bottom portions are not equal. The degree is asymmetry is calculated at Re = 260 by determining the difference in average concentrations at the top and the bottom i.e. $\left|\bar{m}_{A-top} - \bar{m}_{A-bot}\right|$ and is plotted in Fig. 13a. The critical Reynolds number for the engulfment flow is predicted from the degree of asymmetry and is shown in Fig. 13b. As obvious from the Figure, the degree of asymmetry increases, and the critical Reynolds number decrease with an increase in area ratio $R_o$.

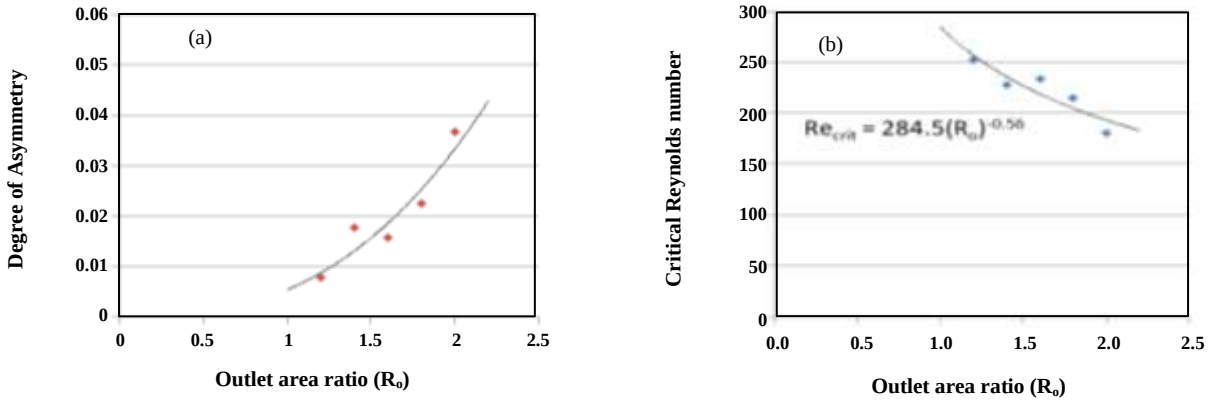


***Fig. 13: Effect of area ratio on (a) the degree of asymmetry (for Re = 260) and (b) the estimated critical Reynolds number.***

The analysis of circulation values, mass fraction contours, mixing quality and critical Reynolds number shows that a mixer channel with a large area ratio $R_o$ is superior in performance. A small ratio of 1.2 for $R_o$, however, can be suggested better in terms of mixing effectiveness for most of the Reynolds numbers. Increasing the inlet area ratio $R_i$ (i.e. $R_i > 1$) is not advantageous as the mixing quality and the effectiveness both are reduced. The micromixer with an inlet area ratio $\approx 1$ can therefore is satisfactory for the micromixer units.

The present numerical work is evaluated with the help of previous results available in the literature. The distribution of mass fraction obtained in this work and the concentration field obtained experimentally by *Hoffmann et al.* [20] is shown in Fig. 14a. The comparison shows the similarity of the mass fraction/concentration profiles. The friction factors are determined from pressure drops using Eq. (14) and are compared with the friction factors obtained in the experimental work of *Aoki et al.* [2]. The plot in Fig. 14b shows that the CFD results through over-predict friction factors; the difference is within 20%. Perfect agreement is not expected due to the accuracy limits of the measurement devices in experiments and numerical errors and uncertainties involved in computational techniques The numerical results are also compared with the work of *Aoki et al.* [3] in which the segregation index was computed using standard deviation ratios at different cross-sections. The comparison of the segregation index versus length or residence time shows that the differences in results are within the acceptable range. The numerical study in this paper, therefore, is found reasonable for the comparison of different micromixer geometries.

## CONCLUSIONS

The flow patterns and mixing rates are determined in narrow channels of micromixers. The effect of cross-section areas of the inlet and the outlet channels are examined on several parameters such as circulation, mixing quality, pressure drop, and mixing effectiveness. The main findings from the research are:

- An increase in the outlet area increases the size of the separation zone which enhances flow recirculation. This flow behavior allows the layers of the fluid to intertwine more which augments the mixing process. The large recirculation zones, but, also lead to increased pressure losses.
- A quantitative comparison of micromixers shows that for most of the Reynolds numbers, mixing quality continuously increases with an increase in outlet area ratio $R_o$. Based on mixing effectiveness (mixing quality divided by Euler number), however, a micromixer with a $R_o$ value of 1.2 is found better than the others.
- The simulations for the effects of inlet area ratio $R_i$ show that both mixing quality and effectiveness are high when $R_i$ is 0.8 or 1.
- From the mass fraction distributions, the flow regimes and the critical Reynolds numbers are predicted. The flow in micromixers is stratified up to Re = 260 when area ratios $R_o$ or $R_i$ are small ($R_o$ or $R_i$ = 0.6). Similarly, the regime is stratified when $R_i = 1.4$. In mixers with $R_o \geq 1.2$, the flow is found to be in the engulfment regime at a high Reynolds number. In the remaining cases, the flows are found in the vortex regime.
- The in-depth analysis of the effect of channel dimensions on mixing efficiency can be useful for the design

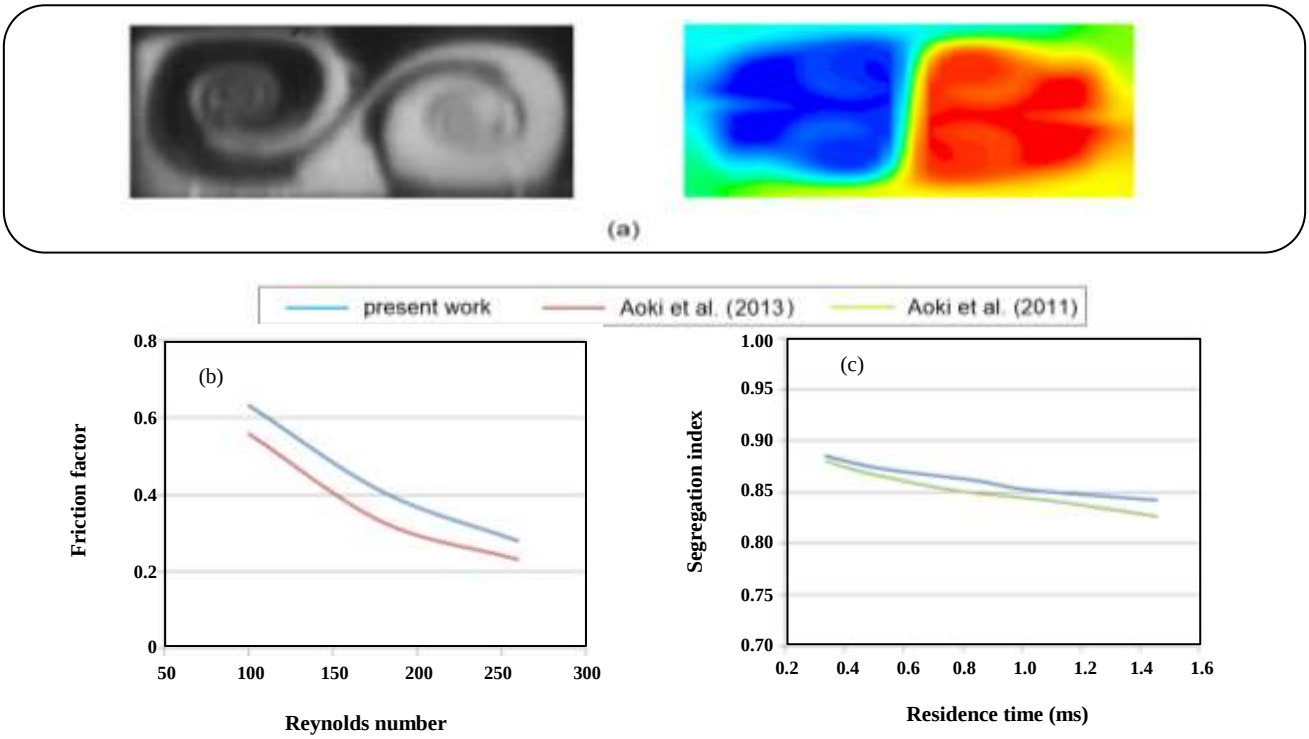


***Fig. 14: Comparison of present numerical simulations ($R_o$ = 2) with (a) experimentally visualized concentration field [20] (b) friction factor from experiments [2] (c) segregation index determined computationally [3].***

of micromixer/microfluidic devices. The Reynolds numbers in practical applications can be higher or lower than those considered in the present work. The effect of diffusion coefficient or Schmidt number also needs to be investigated in detail as it depends on the type of fluid and significantly affects the mixing performance. The research is in progress to simulate the mixing process for various fluids in a wide range of Reynolds numbers.

**Acknowledgment**

The support provided by the NED University of Engineering and Technology, Karachi, Pakistan is acknowledged.

**Nomenclature**

| | |
|---|---|
| $A_i$ | Area of inlet channels, m |
| $A_j$ | Area of micromixer at the junction, m |
| $A_o$ | Area of the outlet channel, m |
| CFD | Computational Fluid Dynamics |
| d | Hydraulic diameter, m |
| $D_{AB}$ | Mass diffusivity, $m^2/s$ |
| Eu | Euler number |
| f | Friction factor |
| h | Height, m |
| $m_A$ | Mass fraction of tracer, kg/kg |
| $\overline{m}_A$ | Mean mass fraction of tracer, kg/kg |
| ME | Mixing Effectiveness |
| Δp | Pressure drop, Pa |
| Re | Reynolds number |
| $Re_{crit}$ | Critical Reynolds number |
| $R_i$ | Area of inlet channels/area of the junction |
| $R_o$ | Area of outlet channel/area of the junction |
| SI | Segregation index |
| u | x-component of velocity, m/s |
| $u_{av}$ | Average velocity, m/s |
| v | y-component of velocity, m/s |
| V | Volume ($m^3$) of the computational domain |
| w | z-component of velocity, m/s |
| $w_{av}$ | Average width, m |
| $w_i$ | Width of inlet channels, m |
| $w_j$ | Width of micromixer at the junction, m |
| $w_o$ | Width of the outlet channel, |
| m | |
| α | Mixing Quality |

| | |
|---|---|
| $\rho$ | Density, kg/m$^3$ |
| $\sigma$ | Standard deviation of mass fraction of tracer, kg/kg |
| $\sigma_0$ | Maximum standard deviation of the mass fraction of tracer, kg/kg |
| $\mu$ | Viscosity, kg/m.s |
| $\nu$ | Kinematic viscosity, m$^2$/s |
| $\omega$ | Circulation, m$^2$/s |

*Received : Oct 5, 2021 ; Accepted : Feb. 14, 2022*

**REFERENCES**


[1] Kockmann N., Kiefer T., Engler M., Woias P., Convective Mixing and Chemical Reactions in Microchannels with High Flowrates, *Sens. Actuators B*, **117 (2):** 495–508 (2006).

[2] Aoki N., Umei R., Yoshida A., Mae K., Design Method For Micromixers Considering Influence of Channel Confluence and Bend on Diffusion Length, *Chem. Eng. J.* **167 (2)**: 643–650 (2011).

[3] Aoki N., Fukuda, T., Maeda, N., and Mae, K. Design of Confluence and Bend Geometry for Rapid Mixing In Microchannels, *Chem. Eng. J.*, **227**: 198–202 (2013).

[4] Kothare M.V., Dynamics and Control of Integrated Microchemical Systems with Application to Micro-Scale Fuel Processing, *Comput. Chem. Eng*., **30 (10)**: 1725–1734. (2006).

[5] Cheri M.S., Latifi H., Moghaddam M.S., Shahraki H., Simulation and Experimental Investigation of Planar Micromixers with Short Mixing Length, *Chem. Eng. J.*, **234:** 247-255 (2016).

[6] Hessel V., Lowe H., Schonfeld F., Micromixers-A Review on Passive and Active Mixing Principles, *Chem. Eng. Sci*., **60(8)**: 2479–2501 (2005).

[7] Jeong G.S., Chung S., Kima C.B., Lee S.H., Applications of Micromixing Technology, *Analyst*, **135**: 460-473 (2010).

[8] Lee C.Y., Fu L.M., Recent Advances and Applications of Micromixer, *Sens. Actuators B*, **259**: 677–702 (2018).

[9] Capretto L., Cheng W., Hill M., Zhang X., Micromixing within Microfluidic Devices, *Top Curr.Chem*, **304**: 27-68 (2011).

[10] Nguyen N-T., Wu Z., Micromixers – A Review, *J. Micromech. Microeng.* **15**: 1–16 (2005).

[11] Shabanian S.R., Masoud M., Abbas K., Alsairafi A., CFD Study on Hydrogen-Air Premixed Combustion in a Micro Scale Chamber, *Iran J. Chem. Chem. Eng. (IJCCE)*, **29(4):**161-172 (2010).

[12] Nazghelichi T., Jafari A., Kianmehr M.H., Aghbashlo M., CFD Simulation and Optimization of Factors Affecting the Performance of a Fluidized Bed Dryer, *Iran J. Chem. Chem. Eng. (IJCCE)*, **32(4):** 81-92 (2013).

[13] Gobby D., Angeli P., Gavriilidis A., Mixing Characteristics of T-Type Microfluidic Mixers, *J. Micromech. Microeng.*, **11(2)**: 126 (2001).

[14] Soleymani A., Kolehmainen E., Turunen I., Numerical and Experimental Investigations of Liquid Mixing in T-Type Micromixers, *Chem. Eng. J.*, **135(1)**: S219-S228 (2008).

[15] Su T., Cheng K., Wang J., A Fast Design Method for Passive Micromixer with Angled Bend, *Microsyst. Technol.* **25:** 4391–4397 (2019).

[16] Darbandi M., Sabouri M., Numerical Study of Mixing Enhancement through Nanomixers Using the Throttling Approach, *Int. J. Sci. Tech*., **22:** 1306-1316 (2016).

[17] Zare P., Talebi S., Gavriilidis A., Numerical Simulation of Geometry Effect on Mixing Performance In L-Shaped Micromixer, *Chem. Engg. Comm*., **207**: 585–597 (2019).

[18] Wong S.H., Ward M., Wharton C.W., Shenoy KT., Micro T-Mixer as a Rapid Mixing Micromixer, *Sens. Actuators B*, **100** (3): 359–379 (2004).

[19] Silva J.P., Sentos A., Semiao V., Experimental Characterization of Pulsed Newtonian Fluid Flows Inside T-Shaped Micromixers with Variable Inlet Widths, *Exp Thermal and Fluid. Sci.*, **89**: 249-258 (2017).

[20] Hoffman M., Schluter M., Rabiger N., Experimental Investigation of Liquidliquid Mixing in T-Shaped Micro-Mixers Using µ-LIF and µ-PIV, *Chem. Eng. Sci*., **61(9)**: 2968–2976 (2006)

[21] Fatima U., Shakaib M., Memom I., Analysis of Mass Transfer Performance of Micromixer Device with Varying Confluence Angle Using CFD, *Chem Pap*., **74**: 1267–1279 (2020).

[22] Shamsoddini R., Numerical Investigation of Fluid Mixing in a Micro-Channel Mixer with Two Rotating Stirrers by Using the Incompressible SPH Method, *Iran J. Chem. Chem. Eng.(IJCCE)*, **36(5)**: 173-183 (2017).

[23] Naher S., Orpen D., Brabazon D., Poulsen C.R., Morshed M.M., Effect of Micro-Channel Geometry on Fluid Flow and Mixing, *Simul. Model. Pract. Theory*, **19**: 1088-1095 (2011).

[24] Alam A., Afzal A., Kim K.Y., Mixing Performance of a Planar Micromixer with Circular Obstructions in a Curved Microchannel, *Chem. Eng. Res. Des*., **92(3)**: 423–434 (2014).

[25] Fang Y., Ye Y., Shen R., Zhu P., Guo R., Hu Y., Wu L., Mixing Enhancement by Simple Periodic Geometric Features in Microchannels, *Chem Eng. J*., **187**: 306–310 (2012).

[26] Wang L., Liu D., Wang X., Han X., Mixing Enhancement of Novel Passive Microfluidic Mixers with Cylindrical Grooves, *Chem Eng. Sci*., **81**: 157–163 (2012).

[27] Kakavandi F.H., Rahimi M., Jafari O., Azimi N., Liquid-Liquid Two Phase Mass Transfer in T-Type Micromixers with Different Junctions and Cylindrical Pits, *Chem. Eng. Process Process Intensif.*, **85**: 58–67 (2018).

[28] Kashid M., Renken A., Kiwi-Minsker L., Mixing Efficiency and Energy Consumption for Five Generic Microchannel Designs, *Chem. Eng. J*., **167(2)**: 436–443 (2011).

[29] Patankar S.V., Spalding D.B., A Calculation Procedure for Heat, Mass and Momentum Transfer in Three-dimensional Parabolic Flows, *Int. J. Heat Mass Transfer*, **15**: 1787–1805 (1972).

[30] Lobasov A.S., Minakov A.V., Kuznetsov V.V., Rudyak V.Y., Shebeleva A.A., Investigation of Mixing Efficiency and Pressure Drop in T-Shaped Micromixers, *Chem. Eng. Process Process Intensif.*, **134**: 105–114 (2018).